Theoretical Characterization of Oxoanion, XO_m^{n-}, Solvation

Donald M. Camaioni,* Michel Dupuis,* and John Bentley†

Pacific Northwest National Laboratory, Chemical Sciences Division, P.O. Box 999, Richland, Washington 99352, and Radiation Laboratory, University of Notre Dame, Notre Dame, Indiana 46556

Received: February 11, 2003; In Final Form: May 3, 2003

We describe a new cavity definition protocol that yields accurate solvation energies and electrode potentials for selected oxoanions, XO_m^{n-}, including some for which other cavity protocols do not perform well enough. In this new definition scheme with cavities made of interlocked atomic spheres, the radii are given by simple empirically based expressions involving effective atomic charges of the solute atoms that fit the solute molecular electrostatic potential and a bond length-dependent factor to account for atomic size and hybridization. The scheme shows substantial qualitative differences from other previously proposed schemes, for example, by assigning a large radius to the central atom of the oxoanions. This difference is put on a firm theoretical basis in the case of NO_3^- through an analysis of the molecular electrostatic potential of the nitrate ion and an analysis of its interaction with a "solvent" water molecule. Despite a large positive partial charge assigned to nitrogen in the nitrate ion, the water solvent molecule continues to act as an H-bond donor in the region of the central N atom as a result of the electrostatic potential of the anion, although the water−nitrate interaction in that region is weaker than near the terminal O atoms. From these results, we surmise that the solvent molecules remain further away from the nitrogen atom, a finding that is consistent with the large radius assigned by the new scheme for nitrogen. The same qualitative feature holds true for all of the oxoanions considered here.

I. Introduction

There is interest in our laboratories in the development of computer models that will allow the characterization of the thermal and radiolytic degradation of high-level wastes (HLW) that are byproducts of nuclear materials processing.[1] Mechanistic probe experiments are being applied to gain fundamental insight into mechanisms that operate during thermal and radiolytic degradation. Concurrently, the methods of computational electronic structure are being applied because they have the potential to provide structural and energetic data that are needed in the models and for which experimental data is either lacking or hard and costly to obtain. The electronic structure and properties of intermediates in aqueous media, including thermochemical properties such as acidity (K_a), redox potentials ($E°$), and reaction energies (ΔH and ΔG), are properties of interest, as are mechanisms and pathways for redox reactions of organic compounds and their rate constants under various conditions. Both experiments and computations aim at obtaining key kinetic data and thermodynamic properties related to thermal reactivity so that rate-controlling and product-forming reactions can be predicted.

Modern computational chemistry provides practical methods that permit calculations of energetics, structures, and properties with near chemical accuracy for reactions involving organics in the gas phase.[2−5] The methods based on functionals of the density[6,7] (DFT), in particular, those that include a contribution from the Hartree−Fock exchange interaction,[8,9] provide simple yet accurate models,[4,5] albeit not quite as accurate as the best wave function-based molecular orbital (MO) theories. Computational protocols such as the G1, G2, and G3 protocols[3−5] have been developed; these are widely followed because of the high likelihood that the calculated data will fall within the estimated accuracy of the model.

Similarly, models of solvation based on a dielectric continuum representation of the solvent[10,11] combined with MO and DFT theories have become widely used to calculate free energies of solvation for solutes in various solvents. Their applications are simple, practical, and computationally inexpensive. For the more elaborate schemes,[12,13] reported mean errors are on the order of a few tenths of a kcal/mole for the test sets of neutral solutes, albeit near ∼4 kcal/mol for the smaller test sets of ions. Unfortunately, in our attempt to apply these models to oxoanions and other ions, we at times experienced errors that were too large in light of the needed accuracy. In part, this may be due to estimates[14] of the hydration energy of the proton that have changed since the development of these models. The hydration energies of ions are tied inextricably to the hydration energy of the proton such that ion energies have also changed.[15] Therefore, to improve our capabilities, we decided to revisit one selected aspect of these models, mainly, the definition of cavities.

I.A. About Dielectric Continuum Models. In the dielectric continuum approaches to solvation, the solute resides inside a cavity carved into the continuum, and the solute−solvent interaction is most often mimicked by partial charges at or near the cavity boundary induced by the electrostatic potential or electrostatic field of the solute molecule. In turn, the induced charges and/or dipoles create an external potential acting on the quantum mechanical solute. This is the self-consistent reaction field (SCRF). Several SCRF models have been

* Corresponding authors. E-mail: donald.camaioni@pnl.gov, michel.dupuis@pnl.gov.
† University of Notre Dame. E-mail: Bentley.1@nd.edu.

10.1021/jp0343537 CCC: $25.00
Published on Web 07/01/2003

developed and implemented in computer programs over the years, including Onsager's SCRF by Rinaldi et al.[16] and Karelson et al.,[17] the polarizable continuum model (PCM) of Tomasi and collaborators,[18] the solvation models (SM5) from Cramer and Truhlar,[19] the conductor-like screening model (COSMO) from Klamt and Schuurmann,[20] the surface and volume polarization for electrostatics model (SVPE) from Chipman,[21] and SS(V)PE methods that simulate SVPE.[22−25] For recent reviews of this field, see refs 10 and 11.

Most modern SCRF methods use a molecule-shaped cavity in contrast to the earlier implementations of Onsager's SCRF that used spherical or ellipsoidal cavities.[16,17] The rationale is that molecule-shaped cavities are more realistic and therefore should yield more accurate free energies of solvation. In many cases, the molecule-shaped cavity is constructed from interlocked spheres with appropriately chosen radii and centered on the atoms. In some cases, the cavity is chosen as a 3D isodensity surface of the electron density.[21] The isodensity-based cavity may be adjusted during the SCRF calculation because the electron density depends on the reaction field from the continuum, which in turn depends on the partial charges and/or dipoles induced at the cavity boundary by the solute electron density. In some respects, it can be argued that an isodensity surface gives an even more realistic representation of a molecular cavity than interlocked spheres because it is a more faithful representation of the molecule. However, hydration of the oxoanion occurs with strong and specific water−solute interactions that may not be simulated well by an isodensity-shaped cavity that does not somehow account for how water interacts with the solute.[41]

I.B. About the Cavity Definition. The main issue associated with these molecule-shaped cavity models is the selection of the atomic radii or the value of the electron density for which the isodensity surface is constructed. In this paper, we use the interlocked sphere cavity model as our starting point. Several suggestions exist for the atomic radii for continuum solvation models. Standard Bondi[26] and Pauling[27] radii scaled by a factor of 1.2 have been used extensively early in the application of these models, although a uniform scaling has been shown to fail at times, as in the case of the glycine zwitterion.[28] Orozco and Luque[29] proposed a uniform scaling of 1.10−1.15 for ions, and Bachs et al.[30] proposed another uniform scaling of 1.20−1.25 for neutral species. Truong and Stefanovich[31] also proposed a modified set of radii to obtain improved agreement with experimental solvation energies for a limited set of molecules, but these radii are not radically different than several of the other suggested radii.[32] Robustness remains elusive for ions for essentially all of the proposed schemes, with regards to providing a consistently high level of accuracy, as noted by Cappelli et al.[33]

Among the various schemes that have been proposed, several of them[13,34−39] include a dependency of the atomic radius on the atomic charge of the atom. The rationale for such an idea can be gained from calculations (using the COSMO model, for example) for small ions O^-, OH^-, and H_3O^+. Default values of the radii originating from the Bondi set[26] yield solvation energies that underestimate the magnitude of the experimental values for these ions. Making the radii smaller greatly improves the calculated free energies of solvation, as is done with the UAHF scheme.[13] This finding is striking and raises questions about the conceptual linkage between radii for solvation calculations and van der Waals' radii. Indeed, the anions are commonly described as "larger" than the neutral parent species, yet the continuum models, at least when the solvent is water, demand smaller radii that make the cavity smaller! In a similar vein, when applying models that use isodensity surfaces to define the solute cavity, anions require a larger value of the density contour than neutral species do to get good "agreement" with experimental results.[40,41] Here again the anions that are commonly described as larger than the neutral parent species require a smaller cavity, and this is simply to increase the strength of the electrostatic response of the continuum medium! These two points are a vivid demonstration of the limitations of schemes based on van der Waals' radii for cavity definition, at least for ions.

We note that perhaps the most widely used set of radii, presumably because of their availability as default values in the Gaussian series of computer codes,[42] is the UAHF set proposed by Barone et al.,[13] as previously mentioned. Their proposal represents one attempt to capture some features of the electronic structure of the solute in the definition of the radii by taking into account, for example, the hybridization state and, in the case of ionic solutes, the formal charge of the solute. In these authors' scheme, larger formal atomic charges, positive or negative, give rise to smaller radii. The "electronic structure" of the solute is interpreted formally however, only in the sense that it is based solely on the chemical formula of the solute. As a result, the fidelity of the "real" electronic structure of the solute can be poor. For ozonide, O_3^-, as an example, the UAHF rules assign $^1/_3$ of an electron to each of the oxygen atoms, and an ab initio population analysis indicates a small positive atomic charge on the central atom and $\sim^1/_2$ of an electron on each of terminal oxygen atom. A similar assignment results in fact from fitting the molecular electrostatic potential with effective atomic charges. Other interesting proposals that capture some aspects of the solute electronic structure are those by Smith and Hall[43] and Das,[44] who suggest defining the solute cavity as the loci of minimum interaction energy between the solute and a probe solvent molecule. Part of our analysis below in support of our own findings will in fact point to the solute−water interaction as an important descriptor for solvation models.

The present research is focused on a single class of species, oxoanions, for which we are in need of predictive and consistent computational capabilities with a high level of accuracy. To this end, we obtained fitted expressions for the atomic radii to reproduce the experimental free energies of solvation for a small training set using the effective atomic charges of the solute atoms that fit the solute molecular electrostatic potential and a bond length-dependent factor to account for atomic size and hybridization. In light of the novelty transpiring from this empirically based protocol, we interpreted our results by establishing a connection between the radii and several aspects of the electronic structure of solute−water complexes. As an example, the new scheme yields a large radius for the central atom in the oxoanions, XO_m^{n-}, under consideration here. We extracted a theoretical basis for this finding in the case of the nitrate ion by characterizing the interaction of a nitrate ion with a water molecule. This analysis is provided below.

I.C. About Standard-State Conventions. Before going into the presentation of our research, it is essential to state at the start the convention used throughout this work with regard to the various contributions included in the calculated free energies of solvation. The ab initio calculations yield the electrostatic contribution in the context of the selected continuum model. Beyond this contribution there is a cavity/dispersion term that represents the energy cost of creating the cavity in the medium and the dispersion interaction of the solute with the solvent.[10,11] Finally, there is a correction term arising from the standard-

state definition in the gas phase and in the solution phase.[45,46] Corrections are required because solvation free energies (ΔG_s*) are computed for the hypothetical process of transferring a species from a fixed position in the gas phase to a fixed position in the solution phase, which is equivalent to using the same standard states for gas and solution phases.[45] However, experimental data typically are reported using different standard states for gases, solutes, and liquids. We use throughout this work the following standard-state definitions: concentrations of gas-phase species are those corresponding to an ideal gas at 1 atm of pressure and 298 K, solutes are in ideal solutions with concentrations of 1 M (298 K), and water is an ideal liquid with a mole fraction of 1. Therefore, ΔG_s* is different from ΔG_s° by −1.9 kcal/mol for solutes and −4.3 kcal/mol for liquid water.[45] As such, the computed free energies of solvation that we discuss in this paper are directly comparable to experimental data. Experimental data used in what follows have been derived from measurements reported in the literature[1b,47−60] and, when needed, from a value of the free energy of solvation of a proton $\Delta G_s°(H^+)$ equal to −264.0 kcal/mol.[14]

In what follows, we describe our new protocol that yields accurate solvation free energies of several oxoanions and related neutral species, including O^-, O_2^-, O_2, O_3^-, NO_2^-, HCO_2^-, NO_3^-, ClO_2^-, O_3, NO_2, CO_2, ClO_2, SO_2 (these as part of the training set), ClO_3^-, ClO_4^-, CO_2^-, CO_3^-, and SO_2^- (these outside the training set). In sections II and III, we describe and discuss the fitting procedure. In sections IV and V, we define the working protocol and demonstrate its performance for oxoanions that are not in the training set. We show that calculated solvation energies using the new empirically based atomic charge/atomic radius relationships lead to more satisfactory agreement with experiment for these species. Our fitted expressions yield radii for the terminal oxygen that get smaller for larger atomic charges. At the same time, these expressions yield radii assigned to the central atoms in these oxoanions that are much larger than those assigned by any other scheme. This is a feature that emerges naturally from the fitting procedure and represents a departure from any other proposal. We discuss in section VI an ab initio characterization of the water−nitrate ion complex in support of this unique feature. The results of these computations substantiate our findings and indicate that our new empirically based scheme embodies some essential features of solute−solvent interactions. We give a summary and conclusions in section VII.

II. Fitting Procedure for New Cavity Definition Scheme

We determined the relationship between atomic charges and radii to fit calculated solvation energies to experiment using an accurate level of theory, mainly spin-unrestricted B3LYP/6-311+G** with the COSMO method[61] (labeled as CPCM in Gaussian 98), using the charge renormalization scheme (ICOMP = 2 in Gaussian 98 nomenclature) that scales the polarization charge by a constant factor to conform with Gauss' law.[62] Note that several correction schemes for charge renormalization exist,[62] and which one, if any, is preferred with which solvation model is debatable.[22,25,41,63] There are suggestions that, in the limit of large dielectric constants, the COSMO method yields results that are nearly equivalent to those of other methods (such as SS(V)PE and the integral equation formalism method) that simulate surface and volume polarization effects.[22,23,25] These methods are equivalent to the SVPE method only when no charge escapes the cavity;[40,63] otherwise, the methods are approximate and require some correction, in particular, for small anions.[40] In any case, detailed calculations with a variety of levels of theory and of renormalization schemes[64] revealed that the 6-311+G**/COSMO-PCM/B3LYP/(ICOMP = 2) level of theory (available both in Gaussian 98 and in HONDO-2002[68]) gave excellent results. Furthermore, two critical findings were first that a renormalization step is imperative (notably for O^- and O_2^-, where charge escaping the cavity is 0.4 to 0.5 of an electron and the renormalization correction amounts to 4 kcal/mol for O_2^- and 8 kcal/mol for O^-; no method was able to produce agreement with experiment for these species without correction) and second that the uniform charge renormalization scaling ICOMP = 2 remains on average within 0.2 kcal/mol and never more than 0.4 kcal/mol away from the supposedly "better" ICOMP = 4 scheme.[63] A detailed discussion of the charge escape data is beyond the scope of this paper. A complete comparative report is in preparation.

A radius scaling factor ALPHA = 1.0 was used throughout in our fitting procedures, whereas the UAHF protocol uses ALPHA = 1.2.[13] Gas-phase structures, optimized at the B3LYP/6-311+G** level, were used initially to define cavity radii that reproduced the experimental hydration free energies. Then, solute geometries were optimized using the solvation model with the corresponding radii. The changes in geometries and the resulting changes in total free energies (including nonelectrostatic contributions) were small and in most cases negligible (Supporting Information). The most notable changes were found for HCO_2^-, ClO_2, and ClO_2^-: −0.6, −0.1, and −0.4 kcal/mol, respectively. Increasing the central cavity radii for these solutes by 0.04, 0.03, and 0.02 Å, respectively, was sufficient to offset these changes and regain agreement with the experimental hydration free energies. The calculations were carried out with the Gaussian-98 code,[42,65,66] the NWChem code,[67] and the HONDO-2002 code.[68] For the Gaussian-98 program, the minimum number of tesserae was set to 576 tesserae/sphere (TSNUM = 576). For HONDO and NWChem, settings of MINBEM = 3 and MAXBEM = 3 were used.

Preliminary calculations of the solvation energy of ozonide led us to consider defining the radii (R_O) of the terminal oxygen atoms in oxoanions as a function of their partial atomic charges (Q_O) as a means to obtain free energies of solvation in close agreement with experiment. These considerations ultimately led to a three-step procedure in which we (1) determined the relationship between the atomic charges (Q_O) of O^-, O_2^-, and O_2 to the O radii (R_O) that reproduce experimental aqueous solvation free energies, (2) used this relationship to fix R_O for terminal oxygens in several polyatomic oxoanions and related neutrals and then determined the radii (R_X) of the central atoms that best reproduce the experimental aqueous solvation free energies, and (3) correlated these R_X values with quantum descriptors (i.e., partial atomic charges (Q_X) and interatomic distances (X−O)). We elaborate each step below.

II.A. Step 1: Determination of the Relationship between Oxygen Radius R_O and Oxygen Charge Q_O. The dependence of the radius of the "terminal" oxygen atom on its partial charge was investigated in the set of three solutes: O^-, O_2^-, and O_2. These systems were selected because a single radius value suffices to define the cavity and partial or atomic charges are unambiguous, equal to −1.0, −0.5, and 0.0, respectively. We adjusted the radii to reproduce the experimental hydration free energies, ΔG_s* = −99.9 ± 0.6, −82.3 ± 1.2, and 2.15 ± 0.02 kcal/mol, respectively, and obtained a satisfactory linear fit (correlation coefficient = 0.994) given in eq 1 and shown in Figure 1.

$$R_O(\text{Å}) = -(0.237 \pm 0.027)|Q_O| + (1.69 \pm 0.03) \quad (1)$$

TABLE 1: Gibbs Free Energies of Hydration (kcal/mol), Cavity Radii (Å), Bond Distances (Å), and Atomic Charges

species	exptl[a]	ΔG_s* e[b]	ΔG_s* ne[c]	R_O[d]	R_X	D_{X-O}	Q_X	$(\partial R/\partial \Delta G_s^*)$[e]
O^-	-99.9 ± 0.6	-101.2	1.3	1.463				0.024
O_2^-	-82.3 ± 1.2	-84.1	1.8	1.558				0.028
O_2	2.15 ± 0.02	-0.2	2.4	1.700				0.13
HCO_2^-[f]	-76.4 ± 2.3	-78.3	1.9	1.47	2.14	1.259	0.872	0.058
ClO_2^-	-67.3 ± 2.1	-72.1	4.8	1.52	2.66	1.634	0.435	0.047
NO_2^-	-69.3 ± 0.6	-72.3	3.0	1.58	2.10	1.264	-0.078	0.11
NO_3^-	-65.0 ± 0.8	-68.1	3.1	1.52	2.40	1.260	1.180	0.059
O_3^-	-71.2 ± 0.7	-74.2	3.0	1.56	2.01	1.352	0.112	0.12
CO_2	0.1 ± 0.01	-2.4	2.5	1.59	2.01	1.161	0.895	0.10
ClO_2	-1.9 ± 0.05	-4.8	2.9	1.60	2.32	1.523	0.746	0.10
NO_2	1.0 ± 0.05	-1.7	2.7	1.67	1.86	1.196	0.194	0.19
O_3	0.8 ± 0.1	-2.0	2.7	1.66	1.73	1.278	0.213	0.21
SO_2	-2.1 ± 0.05	-4.6	2.5	1.61	2.37	1.458	0.697	0.095

[a] For anions from ΔG_f° in Table 2; for neutrals from Henry's law constants in ref 48, except the value for O_3 from ref 70. [b] Electrostatic component of the solvation free energy. [c] Nonelectrostatic component of the solvation free energy. [d] Values (except for O^-, O_2^-, and O_2) obtained from eq 1 using potential-derived (CHELPG) charges for terminal oxygens; see Table 4. [e] Evaluated by single-point calculations of ΔG_s* for values about the value of R_X or R_O in the cases of O^-, O_2^-, and O_2. $\Delta G_s^*(R)$ were fit to a polynomial that was differentiated and evaluated at the value of R_X. These values, multiplied by the uncertainties in the experimental hydration energies, are used to weight the data in multiple linear regression analysis that yielded parameters for eq 2 and fits shown in Figure 2. [f] X = C−H group.

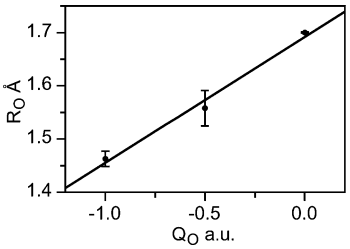

Figure 1. Correlation of cavity radii for O^-, O_2^-, and O_2 with partial charges; see eq 1.

More complex functional forms were found to be unnecessary in light of the accuracy of the fitted data and the quality of the fit given here and below, vide infra.

II.B. Step 2: Determination of R_X in Polyatomic Oxoanions XO_m^{n-} and Related Neutrals. We determined from DFT calculations on a training set of oxoanions (O_3^-, NO_2^-, HCO_2^-, NO_3^-, ClO_2^-, O_3, NO_2, CO_2, ClO_2, SO_2) the partial atomic charges (often referred to as CHELPG charges)[69] that fit the molecular electrostatic potential with the constraint of also fitting the molecular dipole moment (taken with respect to the center of Z atomic charges). The CHELPG charges Q_O on the terminal oxygen atoms yield values of the radii on these atoms, using the expression (eq 1) from step 1. Given the charges and radii of the terminal atoms, we determined the best value for the radius of the central atom X to reproduce the experimental free energy of solvation. Because the presence of the solvent usually induces a change in the electronic charge distribution of the solute, step 2 was iterated until there were no significant variations in the CHELPG charges. In practice, we found that at most only two passes were needed. Table 1 lists the experimental energies along with the CHELPG charges and radii that reproduce the experimental energies using COSMO-PCM (B3LYP/6-311+G**, scaling factor ALPHA = 1.0, ICOMP = 2). Uncertainties in the experimental hydration energies were explicitly taken into account by the fitting program (proFit, QuantumSoft, Zurich, Switzerland). Numerically determined derivatives of the calculated hydration energies with respect to R_X are shown in Table 1. These were multiplied by the uncertainty in the hydration energy to obtain the uncertainty in R_X. The uncertainties estimated in this way for the anions are in the range $0.05 \le \Delta R_X \le 0.13$ Å. The uncertainties in the hydration energies of the neutrals are much smaller than for anions. Because the radii that are used are rounded to two decimals, we assigned the errors for neutrals as $\Delta R_X = 0.005$ Å.

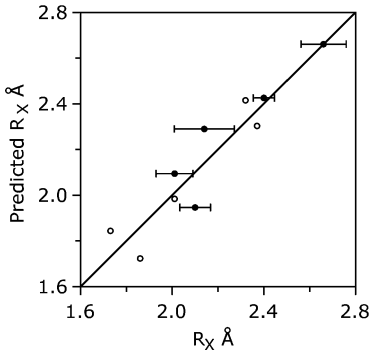

Figure 2. Cavity radii for central atoms/C−H group in (●) anions and (○) neutrals predicted by eq 2 plotted against radii that reproduce experimental hydration energies. From left to right, the points are O_3, NO_2, CO_2, O_3^-, NO_2^-, HCO_2^-, ClO_2, SO_2, NO_3^-, and ClO_2^-. The line represents a one-to-one correspondence. Error bars are the products of the uncertainty in the experimental solvation energy and $(\partial R_X/\partial \Delta G^*_s)_{R_O}$.

II.C. Step 3: Relationship between Radius R_X and Charge Q_X and Distance X−O. The best radii for the central atoms (denoted X) obtained in step 2 were fitted to a function in which the CHELPG charge on the central atom, Q_X, and the distance between the central atom and the terminal oxygen atoms, D_{X-O},were variables:

$$R_X(\text{Å}) = (0.44 \pm 0.01)|Q_X| + aD_{X-O} \qquad (2)$$

where $a = 1.37$ for neutrals or 1.51 ± 0.03 for anions.

Figure 2 compares the radii for central atoms predicted by eq 2 with the actual radii. The points trend with the line for a one-to-one correspondence. No trend is evident when the radii are correlated with either D_{X-O} or Q_X alone.

Figure 3 compares the ΔG_s* calculated using radii predicted by eqs 1 and 2 with experimental values. For neutrals, the hydration energies are predicted to within 1 kcal/mol. The fit to anions is within the experimental errors except for that to the formate ion. The source of the lower accuracy for the formate ion could be in our using a united-atom representation of the CH group or in the gas-phase ion energetics for formate. In Table 1, we show the electrostatic and nonelectrostatic components of ΔG_s* that are generated by the Gaussian-98 CPCM program. Their sum corresponds to the total hydration free energy to which we fitted the radii. For the neutrals, the

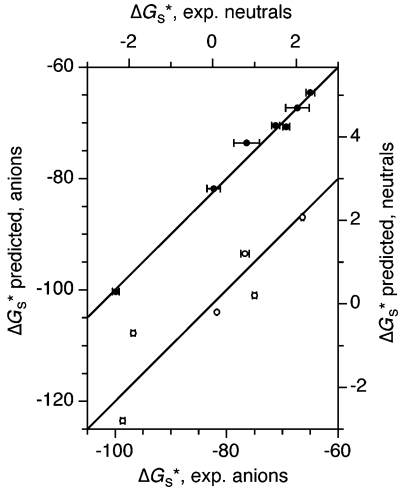

Figure 3. Experimental hydration free energies (kcal/mol) calculated using radii from eqs 1 and 2: (●) anions, bottom and left axes and (○) neutrals, top and right axes. From left to right, the points are (anions) O^-, O_2^-, HCO_2^-, O_3^-, NO_2^-, ClO_2^-, and NO_3^- and (neutrals) SO_2, ClO_2, CO_2, O_3, NO_2, and O_2. Lines represent one-to-one correspondences.

TABLE 2: Experimental Free Energies of Formation (kcal/mol) for Gas and Aqueous Phases

species	$\Delta G_f°$ 298 K, 1 atm	note	species	$\Delta G_f°$ 298 K, 1 M	note
HCO_2^-	-109 ± 2	*a,b*	HCO_2- (aq)	-85.0 ± 0.2	*c*
ClO_2^-	-25.4 ± 1.4	*a,d*	ClO_2^- (aq)	7.7 ± 0.7	*e*
H^+	362.6	*a,g*	H^+ (aq)	0	*h*
NO_2^-	-39.6 ± 0.2	*a*	NO_2^- (aq)	-8.4 ± 0.4	*i*
NO_3^-	-62.0 ± 0.7	*a,d*	NO_3^- (aq)	-26.5 ± 0.1	*f*
O^-	21.9 ± 0.2	*a*	O^- (aq)	22.5 ± 0.4	*j*
O_2^-	-10.7 ± 1	*a*	O_2^- (aq)	7.5 ± 0.1	*k*
O_3^-	-10.8	*a,d*	O_3^- (aq)	18.4 ± 0.1	*a,l*

[a] Ref 48. [b] $\Delta G_f°(HCO_2H) = -90.1 \pm 2$; $\Delta G_a° = 338 \pm 2$. [c] $pK_a(HCO_2H) = 3.751$, $K_h(HCO_2H) = -5.4 \pm 0.2$. [d] $S°$ from the B3LYP/6-311+G** frequency calculation. [e] From $E°(ClO_2/ClO_2^-) = 0.934 \pm 0.002$ V.[52] [f] Ref 49. [g] Ref 53. [h] Assigned value; absolute value 98.6 kcal/mol from $\Delta G_f°(H^+(g))$ following the ion convention[53] and $\Delta G° = 264.0$ kcal/mol[14] for the hydration of the proton. [i] From $\Delta G_f°(NO_3^-(aq))$ and $E°(NO_3^-/NO_2^-) = 0.01$ V.[55] [j] From $\Delta G_f°(OH(aq)) = 6.2 \pm 0.2$ and $pK_a = 12$.[52,50] [k] From $E°(O_2/O_2^-) = -0.325 \pm 0.005$ V. [l] Ref 52.

nonelectrostatic hydration free energy is a significant part of the hydration free energy such that further improvements in accuracy would depend on improving that part of the model.

III. Comparative Results for Oxoanions in the Training Set

We carried out benchmark calculations of standard free energies of hydration for anions and neutral oxides of carbon, nitrogen, sulfur, and chlorine (O^-, O_2, O_2^-, O_3^-, NO_2^-, HCO_2^-, NO_3^-, ClO_2^-, O_3, NO_2, CO_2, ClO_2, and SO_2), including comparisons with the SM5 solvation model[11] and the COSMO solvation models.[20] The results including the experimental values are given in Table 3.

The free energies in solution include the electrostatic solute/solvent interaction and the nonelectrostatic cavity terms. The zero-point energy correction, the thermal corrections, and the entropy corrections to the solvation energy were not made because the geometries barely changed when the structures were optimized in the aqueous environment, for example, using the COSMO model. The UAHF radii topology,[13] although originally devised for the PCM solvation model in conjunction with the Hartree−Fock (HF) level of theory, has the characteristic feature that it accounts in part for the chemical functionalities in the molecule. Indeed, the UAHF topology uses van der Waals' radii modified according to the atom types, their formal charges if the solute is an ion, and the number of attached hydrogen atoms. For example, the radius associated with a carbonyl oxygen is different than the one associated with an alcohol oxygen. Atoms carrying a formal charge have different radii than atoms of the same element with no formal charge. In many ways, the parameter fitting of the SM5 solvation model also accounts for the specificity of the electronic structure of the solute and solvents, although the user does not have control over the atomic radii used in the model.

The COSMO-PCM/UAHF approach yields absolute hydration energies of varying accuracy, although they are somewhat better than those of the SM5 model. For the neutral species, COSMO-PCM/UAHF gives values that are on average ~1 kcal/mol too negative. For the ions, the errors are sometimes larger, especially for anions that are small or highly localized (e.g. O^-, O_2^-, CH_3O^- (−91.7 calculated compared to −95.2 kcal/mol[15] from experiment), and OH^- (−111 calculated compared to −105 kcal/mol from experiment[15])). It is worth emphasizing that these errors are 1 order of magnitude larger than the changes obtained from the use of the suggested "better" charge renormalization scheme ICOMP = 4. The results essentially hold, whether the hydration energies are calculated at the gas-phase optimized structures or using the structures optimized in their respective phases. The errors discussed above lead to large errors for acid−base reaction energies, for example, and therefore to unrealistic pK_a and redox potentials.

We recognize that, because the UAHF protocol was conceived as a "general" procedure for a large variety of mainly organic compounds, our new protocol, with its focus on a single class of structurally related oxoanions and neutrals, should yield more accurate results. However, we emphasize that the choice of eq 1 for the definition of the radii of the terminal oxygen atoms leads to a significant departure from the UAHF and other protocols. It can be seen that, when eq 2 is combined with eq 1, the radii of the central atoms in the oxoanions and neutrals increase with the magnitude of the charge assigned to the central atoms X. In contrast, the UAHF protocol reduces the radius for X in oxoanions by a factor equal to 0.3 times the formal charge on X. For example, in the case of ozonide O_3^-, UHAF assigns $^1/_3$ of an electron to each of the three oxygens. Table 4 compares radii developed by our new protocol with the UAHF radii. Overall, our radii are significantly different than the UAHF values, being dramatically smaller for the terminal oxygen atoms and, in many of the anions, much larger for the central atoms.[72] Despite these marked differences in radii, the solvation energies are in good accord with the largest discrepancies arising when charges are strongly localized (O^- and O_2^-).

These observations caused us to question whether eqs 1 and 2 are consistent with the "physics of solvation". In section VI below, we examine this question by analyzing the calculated nitrate ion−water molecular interactions. The conclusions from this analysis are that our new protocol is indeed more consistent with the fundamental chemical interactions that govern oxoanion solvation than other solvation protocols.

IV. Empirically Derived Protocol

On the basis of the fitting procedure described above, the protocol to predict accurate free energies of solvation involves the following steps:

(1) Calculate the equilibrium structure of a given oxoanion using the DFT (B3LYP/6-311+G**) level of theory, and extract the CHELPG charges.

TABLE 3: Free Energy of Solvation ΔG_s* (kcal/mol) from the SM5 Model and from the COSMO-PCM Model Using UAHF Radii and Radii from This Work

species	SM5[a] HF/6-31+G*	SM5[a] BPW91/6-31G*	COSMO UAHF[b] HF6-31+G*	COSMO UAHF[b] B3LYP/6-311+G**	this work[c]	exptl
CO_2	1.7	0.0	−0.5	0.1	−0.2	−0.1 ± 0.01
CO_2^-	−73.8	−74.6	−67.9	−65.3	−67.9	
HCO_2^-	−74.1	−74.9	−77.1	−73.1	−73.6	−76.4 ± 2.3
CO_3^-			−61.3	−61.8	−63.1	
CO_3^{2-}	−277.1	−278.4	−251.8	−257.8	−243.1	
ClO_2	−22.5	−16.5	−2.7	−2.2	−0.7	−1.9 ± 0.05
ClO_2^-	−91.4	−85.6	−68.5	−67.7	−67.3	−67.3 ± 2.1
ClO_3^-	−84.2	−83.0	−63	−62.5	−62.5	
ClO_4^-	−68.4	−74.8	−56.1	−56.5	−54.1	
NO_2	−0.6	−0.7	−1.4	−1.0	0.2	1.0 ± 0.05
NO_2^-	−74.8	−75.6	−66.8	−66.3	−70.7	−69.3 ± 0.6
NO_3^-	−69.2	−68.8	−63.8	−63.1	−64.4	−65.0 ± 0.8
NO_3^{2-}			−262.1	−260.0	−267.0	
O^-	−107	−107.8	−104.1	−101.2	−100.3	−99.9 ± 0.6
O_2	0.8	−7.0	1.4	1.3	2.1	2.1 ± 0.02
O_2^-	−90.3	−93.7	−78.7	−77.8	−81.8	−82.3 ± 1.2
O_3	−5.0	−9.8	0.6	−0.3	1.2	0.7 ± 0.1
O_3^-	−80.6	−85.6	−70	−68.8	−70.5	−71.2 ± 0.7
SO_2	−10.8	−13.0	−4.3	−3.2	−2.8	−2.1 ± 0.05
SO_2^-		−84.3	−68.5	−66.3	−67.9	
muse[d]	7.7	8.5	1.6	1.7	0.8	

[a] Calculations performed with code HONDO/S-2.0.[71] [b] Calculations performed with code Gaussian 98 CPCM default UAHF radii (ALPHA = 1.2, ICOMP = 2).[42] [c] Radii derived from eqs 1 and 2. [d] Mean unsigned errors compared to experiment.

SCHEME 1: Thermochemical Cycle That Shows How Gas- and Aqueous-Phase Redox Reactions Are Related by the Solvation of Reactants and Products

$$\begin{array}{ccc} & \Delta G^\circ_r & \\ Ox^{+m}(g) + ne^-(g) & \rightleftarrows & Red^{-n+m}(g) \\ \downarrow\uparrow \Delta G^\circ_s(\text{reactants}) & & \downarrow\uparrow \Delta G^\circ_s(\text{products}) \\ & E^\circ & \\ Ox^{+m}(aq) + ne^-(g) & \rightleftarrows & Red^{-n+m}(aq) \end{array}$$

TABLE 4: Bond Distances, CHELPG Partial Charges, and Cavity Radii for Species

		partial charge		radii (this work)[a]		UAHF radii[b]	
species	D_{x-o}	O	X	O	X	O	X
CO_2	1.161	−0.448	0.895	1.59	1.98	1.908	2.124
CO_2^-	1.231	−0.397	0.205	1.60	1.95	1.788	2.004
HCO_2^-[c]	1.252	−0.938	0.876	1.47	2.29	1.62	2.232
CO_3^-	1.273	−0.722	1.168	1.52	2.44	1.926	1.818
CO_3^{2-}	1.308	−1.204	1.613	1.41	2.68	1.728	1.8
ClO_2	1.523	−0.367	0.735	1.60	2.41	1.908	2.376
ClO_2^-	1.634	−0.717	0.435	1.52	2.66	1.788	2.256
ClO_3^-	1.542	−0.584	0.752	1.55	2.67	1.818	2.286
ClO_4^-	1.501	−0.578	1.311	1.55	2.84	1.836	2.304
NO_2	1.196	−0.102	0.205	1.67	1.72	1.908	1.8
NO_2^-	1.264	−0.453	−0.094	1.58	1.95	1.908	1.56
NO_3	1.234	−0. 295	0.886	1.62	2.08	1.908	1.8
NO_3^-	1.260	−0.728	1.184	1.52	2.43	1.818	1.74
NO_3^{2-}	1.344	−0.787	0.362	1.50	2.19	1.728	1.68
O^-		−1		1.45		1.44	
O_2		0		1.69		1.854	
O_2^-		−0.5		1.57		1.728	
O_3	1.278	−0.104	0.208	1.66	1.84	1.854	1.692
O_3^-	1.352	−0.542	0.083	1.56	2.09	1.788	1.68
SO_2	1.458	−0.351	0.702	1.61	2.30	1.908	2.376
SO_2^-	1.542	−0.628	0.256	1.54	2.45	1.788	2.256

[a] Radii derived from eqs 1 and 2. [b] Includes a scale factor of α = 1.2. [c] X = CH.

(2) Apply eqs 1 and 2 to get the radii for the terminal oxygen atoms and the central atom from the knowledge of the partial charges, the total charge of the species, and the X−O distance.

(3) Carry out a COSMO(ICOMP = 2, ALPHA = 1.0)/B3LYP/6-311+G** calculation of the free energy of solvation, and extract the CHELPG charges for the solvated wave function. With the new charges, go back to step 2. The iterative procedure is repeated until there are no significant changes in the CHELPG charges. For most cases, two iterations will suffice.

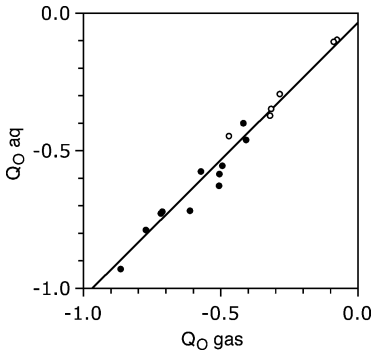

Figure 4. CHELPG charges of the terminal oxygen atoms in aqueous medium vs those in the gas phase for the anions (●) and for the neutrals (○). The solid line corresponds to $Q_O(aq) = Q_O(gas) - (0.03 \pm 0.01)$ au.

(4) Finally, reoptimize the structure using the solvation model and radii as defined thus far. If the energy and/or charges change enough to affect the radii by more than 0.01 Å, then the process is repeated from step 2.

The above protocol is iterative. An abbreviated protocol would involve no iterations (i.e., with the gas-phase CHELPG charges simply determining the atomic radii according to eqs 1 and 2). Figure 4 plots the CHELPG charges of the terminal oxygen atom in solution versus CHELPG charges in the gas phase. The solution CHELPG charges are found to be ∼0.03 au more negative than the gas-phase CHELPG charges. This finding establishes that one can use the gas-phase CHELPG charges in connection with eqs 1 and 2 without iterating. Iterating would be warranted if the solution CHELPG charges fall outside the tolerances for the equations.

V. Applications to Oxoanions outside the Training Set

We applied the above protocol to several oxoanions outside the training set. These included CO_2^-, CO_3^-, CO_3^{2-}, NO_3^{2-},

TABLE 5: Comparison of Predicted and Experimental Reduction Half Reactions of Oxoanions and Neutrals[a]

	$\Delta G_r°$(g) kcal/mol				$E°$ (aq) V vs SHE[b]			
reduction half-reaction	exptl[c]	B3LYP/ 6-311+G**	B3LYP/ a-pVTZ[d]	G3B3	B3LYP/ 6-311+G**	B3LYP/ a-pVTZ[d]	G3B3	exptl
$CO_2(g) + e^- = CO_2^-(aq)$		5.8	6.5	13.5	−1.70	−1.74	−2.00	−1.90[e]
$CO_2(g) + H^+(aq) + 2e^- = HCO_2^-(aq)$	−376.5	−380.9	−380.4	−376.2	−0.22	−0.24	−0.29	−0.219[f]
$CO_3^-(aq) + 2H^+(aq) + e^- = CO_2(g) + H_2O(l)$		−736.4		−747.1	2.16		2.65	2.65[g]
$CO_3^-(aq) + 2H^+(aq) + 2e^- = CO_2^-(aq) + H_2O(l)$		−730.6		−733.8	0.23		0.33	0.38[h]
$CO_3^{2-}(aq) + 3H^+(aq) + 2e^- = HCO_2^-(aq) + H_2O(l)$		−1202.4		−1202.6	0.96		0.96	0.318[i]
$NO_2(g) + e^- = NO_2^-(aq)$	−51.9	−52.8	51.1	−52.0	0.96	0.88	0.95	0.90[j]
$NO_3(aq) + e^- = NO_3^-(aq)$	−89.7	−88.9		−89.8	2.39		2.46	2.3−2.6[k]
$NO_3^-(aq) + e^- = NO_3^{2-}(aq)$		138.3		145.1	−1.54		−1.79	−0.9[l]
$ClO_2(g) + e^- = ClO_2^-(aq)$	−54.7	−57.4	−51.3	−49.6	0.99	0.72	0.68	0.934[m]
$ClO_3^-(aq) + 2H^+(aq) + e^- = ClO_2(g) + H_2O(l)$		−730.5	−723.0	−712.9	1.93	1.60	1.20	0.89[n]
$ClO_3^-(aq) + 2H^+(aq) + 2e^- = ClO_2^-(aq) + H_2O(l)$		−787.8	−774.3	−762.5	1.46	1.16	0.94	0.91[o]
$ClO_4^-(aq) + 2H^+(aq) + 2e^- = ClO_3^-(aq) + H_2O(l)$		−798.3	−788.2	−775.2	1.78	1.55	1.30	1.24[p]
$SO_2(g) + e^- = SO_2^-(aq)$	−26.2	−38.2	−34.9	−25.6	0.21	0.06	−0.31	−0.30[q]
$H^+(aq) + e^- = {}^1/_2H_2(g)$	−361.7	−363.4	−363.5	−362.8	0[e]	0[e]	0[e]	0[r]
mean unsigned errors[s]		3.7	4.5	1.2	0.36	0.17	0.10 (0.05)	

[a] Gas-phase free energies ($\Delta G°$) and aqueous-phase electrode potentials ($E°$). Standard states: gas phase, 298 K, 1 atm; solution phase, 298 K, 1 M (solutes), 1 mole fraction (liquid water). [b] From eq 5, where F is Faraday's constant (23.06 kcal/mol•e$^-$), n is number of electrons transferred in the half reaction, $G°(e^-, gas) = -0.87$ kcal/mol,[53] and $G°(H^+, gas) = -6.3$ kcal/mol. Solvation energies obtained from the Gaussian98 COSMO−polarizable continuum model using B3LYP/6-311+G** gas-phase optimized geometry, ICOMP=2 charge renormalization and radii predicted with eqs 1 and 2, except $\Delta G_s°(H^+) = -264.0$ kcal/mol,[14] $\Delta G_s°(H_2O) = -2.05$ kcal/mol. [c] Derived from standard heats of formation and standard entropies from ref 48 except that entropies for ClO_2^-, NO_3^-, and O_3^- are from B3LYP/6-311+G** frequency calculations. [d] B3LYP/AUG-cc-pVTZ//B3LYP/6-311+G**. [e] ref 54. [f] From $E°[CO_2(g)HCO_2H(aq)] = -0.20$ V and $pK_a = 3.751$ for HCO_2H.[55] [g] From $E°[CO_3^-(aq)/CO_3^{2-}(aq)]=1$ V.[56] [h] From $E°[CO_2(g)/CO_2^-(aq)]$ and $E°[CO_3^-(aq)/CO_3^{2-}(aq)]$, entries 1 and 3 of this table. [i] From entry 2 and $\log K = 16.69$ for $CO_2(aq) + H_2O(l) = CO_3^{2-} + 2H^+(aq)$[55] and $K_H(CO_2) = 0.034$ M/Atm.[48] [j] From $E°[NO_2(aq)/NO_2^-(aq)] = 1.03$ V[57] and $K_H = 0.007$ M/Atm.[48] [k] ref 58. [l] ref 1b. [m] ref 52. [n] From $E°[ClO_4^-(aq)/ClO_2(g)]$ and $E°[ClO_4^-(aq)/ClO_3^-(aq)]$. [o] From $E°(ClO_2/ClO_2^-)$, $E°(ClO_2/ClO_4^-)$ and $E°(ClO_3^-/ClO_4^-)$. [p] ref 60. [q] ref 59. [r] Assigned value. Absolute potential is 4.24 V based on the $\Delta G_f°(H^+) = 361.7$ kcal/mol (electron convention Fermi-Dirac statistics)[53] and $\Delta G_s°(H^+) = -264.0$ kcal/mol.[14] Absolute potentials computed with B3LYP/6-311+G**, B3LYP/AUG-cc-pVTZ and G3B3 are 4.31, 4.32, and 4.28 V, respectively. Differences are due to differences in the values for $G°(H_2)$ calculated by these methods. [s] Excluding reactions involving dianions and, in parentheses, reactions involving ClO_2; note the calculated values for gas-phase electron affinity of ClO_2 is 5 kcal/mol compared to ≤1 kcal/mol for the other species.

SO_2^-, ClO_3^-, and ClO_4^-. The hydration energies of these species cannot be obtained from experimental data because gas-phase free energies of formation are lacking. Accurate redox potentials of reactions involving these species are available in the literature. Therefore, we computed $E°$ for electrode half-reactions that link the above species with one of the ions or neutrals from the training set. These are shown in Table 5 along with electrode reactions (entries 3, 5, and 9) that involve only species within the training set.

The reactions are of the form

$$Ox^{+m}(aq) + ne^- \rightleftarrows Red^{-n+m}(aq) \qquad (3)$$

for which the potential is defined as $E = -\Delta G/(nF)$ where F is Faraday's constant (23.06 kcal/mol•e$^-$/V).

The $E°$ values in Table 5 are referenced to the standard hydrogen electrode (SHE) half-reaction, eq 4, which is assigned a value of 0 V.

$$2H^+(aq) + 2e^-(g) \rightleftarrows H_2(g) \qquad (4)$$

However, the absolute potential of eq 4 is 4.24 V,[53] so this amount is subtracted from the potentials computed for eq 3. We calculated the potentials using the thermodynamic cycle shown in Scheme 1. It involves the gas-phase (electron attachment) reaction and hydration reactions of reactants and products, which leads to an expression for $E°$ given by eq 5.

$$E° = \frac{-[\Delta G_r°(gas) + \Sigma\Delta G_s°(products) - \Sigma\Delta G_s°(reactants)]}{(nF) - E_4} \qquad (5)$$

where the standard states refer to 298 K and 1 atm for gas-phase reagents, 1 M for aqueous solutes, and a mole fraction of 1 for liquid water. We do not solvate the electron because the process cancels out when the potential of eq 3 is referenced to the SHE potential. In some of the reactions, water or protons are consumed or produced. In these cases, we used the experimental values for the free energy of water condensation (eq 6) and the hydration free energy of a proton (eq 7), respectively, so that errors are limited to the species of interest.

$$H_2O(g) \rightleftarrows H_2O(l) \qquad \Delta G_6° = -2.05 \text{ kcal/mol}^{55a} \qquad (6)$$

$$H^+(g) \rightleftarrows H^+(aq) \qquad \Delta G_7° = -264.0 \text{ kcal/mol} \qquad (7)$$

From eq 5, it is evident that the accuracy of the calculation depends on calculating the energies for the gas-phase reaction and the hydration of the reactants and products accurately. The gas-phase reaction free energies were calculated in three different ways: (1) using the B3LYP functional with the 6-311+G** basis set; (2) using the B3LYP functional with the aug-cc-pVTZ basis set; and (3) and using the empirically corrected ab initio G3B3 protocol with the inclusion of thermochemical corrections to 298 K and 1 atm of pressure. Hydration free energies were calculated in the same manner as for the training set, using B3LYP/6-311+G** optimized gas-phase geometries and COSMO-PCM with cavity radii defined by eqs 1 and 2.

The results in Table 5 generally show close agreement beween the calculated $E°$ values and those from experiment for the monoanions when the G3B3 method is used to calculate the gas-phase reactions energies, although poor agreement is obtained for one-electron reduction potentials involving ClO_2. This may be traced to the poor performance of G3B3 in calculating the gas-phase reactions of ClO_2; for example, the

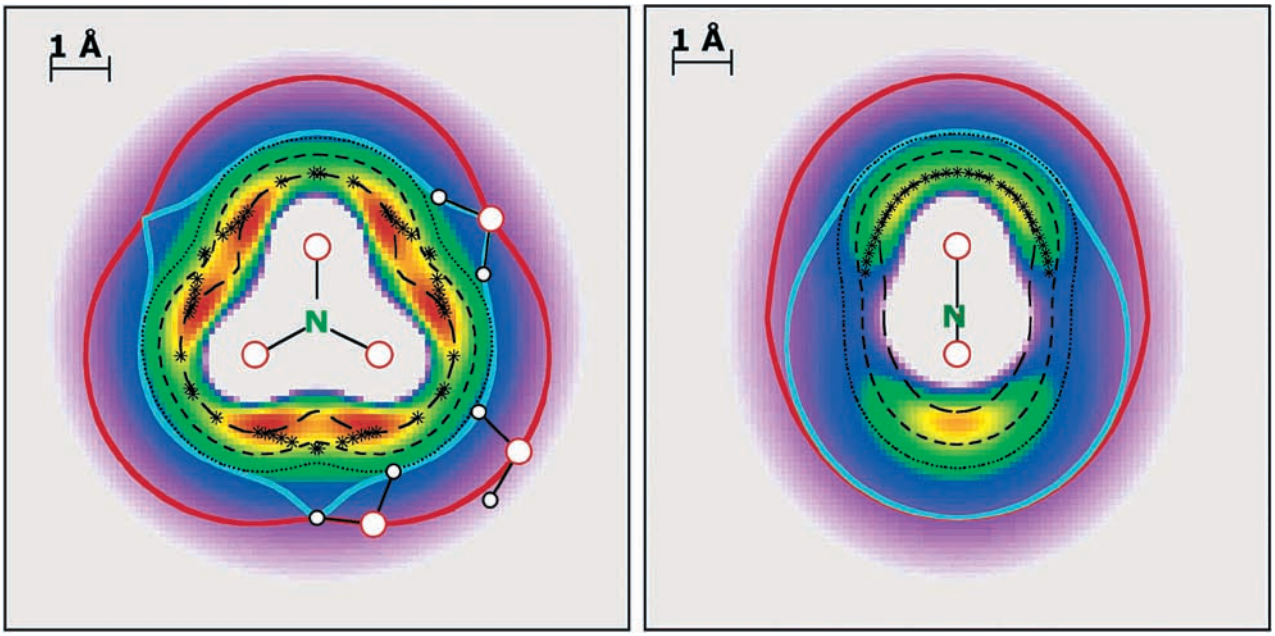

Figure 5. Electrostatic potential contours, electron isodensity contours, and minimum interaction energy (MIE) nitrate−water contours for NO_3^- (left) in the molecular plane and (right) perpendicular to the molecular plane along one N−O bond. Electron isodensity contours values: (•••) 5×10^{-4}, (- - -) 2×10^{-3}, (− − −) 1×10^{-2} e^-/au^3. Electrostatic isopotential contour values for unit positive test charge (kcal/mol): (light gray) ≥−75, (dark purple) −94, (dark blue) −113, (dark green) −132, (yellow) −151, (red) −169; (*) H-bond critical points; (red lines) water−oxygen MIE surface; (light-blue lines) water−hydrogen MIE surface.

electron affinity (Table 5) differs from experiment by ∼5 kcal/mol. Larger errors of ∼1 V in the aqueous reduction potential are obtained in the calculation of dianions. Although the problem here may reside in poorly calculated gas-phase energies for dianions, we do not rule out the possibility that eqs 1 and 2 may not be applicable to dianions.

VI. Nitrate−Water Interaction and the Implication for Aqueous Solvation

In support of the qualitative trends observed with the newly presented protocol that suggests a large radius for the central atom of the oxoanions, we carried out a computational characterization of the electronic structure of the nitrate ion, including B3LYP/6-311+G** calculations of the electrostatic potential (ELP) of the ion. Note that the Mulliken population analysis of the Kohn−Sham DFT wave function assigns a partial charge of +0.65 to nitrogen and −0.55 to each oxygen atom. The CHELPG charges are +0.92 and −0.64, respectively. These partial charges are to be contrasted with the formal charges of 0.0 for nitrogen and −0.33 for oxygen assigned by the UAHF scheme. ELP contour plots in the plane of the molecule and in the plane perpendicular to the molecular plane passing through nitrogen and one oxygen atom are displayed in Figure 5.[76]

The ELP contours in the molecular plane show clearly the lone pair sites on the oxygen atoms. There are six of these sites, and they are sites of strongest electrostatic interaction. Beyond these sites lies a region of lesser electrostatic interaction (∼40 kcal/mol for a unit positive test charge) that surrounds the molecule. The electrostatic potential slowly decreases further in a spherical region away from the ion. The ELP displays the 3-fold symmetry of the molecule.

In the perpendicular plane, the upper portion contains an oxygen nucleus, and in that region the ELP is strong. At the opposite end, the plane bisects two NO bonds, and there is also a region of strong ELP. It is striking that there is an ELP hole in the regions above and below the nitrogen atom where the ELP is ∼60 kcal/mol weaker than in the region around the oxygen atoms. At large distances, the ELP corresponds to a nearly spherical envelope surrounding the ion.

The interaction of a water molecule with nitrate is governed to a very large extent by electrostatic interactions. Ebner et al.[77] calculated HF/6-311+G** energies for a large number of nitrate−water configurations. These authors obtained an analytical expression representing the 3D surface of interaction. These authors report that when the water molecule approaches nitrate in the region above the nitrogen atom an attractive interaction energy is obtained only when the water molecule approaches nitrate with one of the hydrogen atoms first, and a repulsive interaction is observed when the water oxygen atom approaches closest to nitrate. This observation is corroborated by the observation made above that, despite the large partial atomic (Mulliken or CHELPG) charge assigned to nitrogen, there is no region of positive ELP anywhere around the nitrate ion. As a consequence, the interaction of a water molecule with nitrate will be as a hydrogen bond donor from everywhere in space. Special cases of the nitrate−water interaction are those corresponding to (local) minima in which a water molecule attaches to a lone pair of one of the oxygen atoms, as shown first in the work of Ebner et al.[77] and recently in the work of Wang et al.[78]

Also displayed in Figure 5 are the isodensity contours corresponding to the density values of 5×10^{-4}, 2×10^{-3}, and 0.01 e/au^3. It can be noted that in either one of the cut planes the isodensity contours follow the shape of the ELP contour, except in regions around nitrogen above and below the molecular plane and bisecting the O−N−O angle where the isodensity contours hug the molecule much more than the ELP contour does. A consequence of using an isodensity surface as the cavity boundary is that it allows the charges induced in this region of the dielectric continuum to reside much more closely to the nitrate ion than a solvent water molecule could approach on the basis of the ELP.[79] The same observation applies to the cavity defined on the basis of the UAHF protocol. The cavity is ∼0.7 Å closer to N compared to the cavity defined by this work. (See data for the nitrate ion in Tables 1 and 3.) The closer

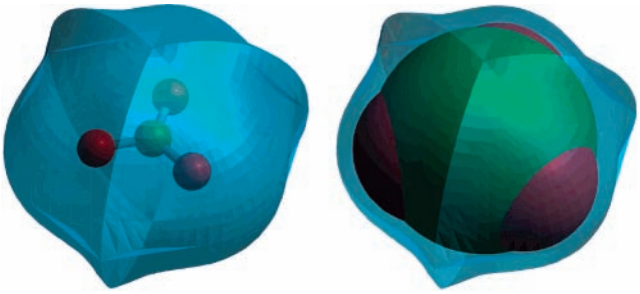

Figure 6. Three-dimensional representations of the H surface corresponding to the minimum interaction energy surface for nitrate−water showing on the inside (left) the nitrate ion and (right) the dielectric continuum cavity using radii from eqs 1 and 2.

approach of the continuum in isodensity and UAHF models is offset by their tendency to place the cavity further from the oxygen (∼0.1 and 0.3 Å, respectively). These features must be a source of canceled errors.

Neither of the studies of the nitrate−water system by Ebner et al.[77] and by Wang et al.[78] shows a local minimum interaction energy structure where the water molecule would bind to nitrate above or below the nitrogen atom. The ELP contours of Figures 5 and 6 are consistent with the findings by these authors. We can then ask the question, How close to the nitrate ion can a water molecule come? Along the line of work by Smith and Hall,[38] we generated a 3D surface of minimum interaction energy (MIE) for the nitrate−water system. To this end, we used the interaction potential developed by Ebner et al.[77] Assuming that nitrate lies in the (x, y) plane with N at the origin, we define many directions on a unit sphere by means of the Euler angles (θ, φ). For a given direction, we determine the distance $R(\theta, \varphi)$ of the position of the oxygen atom of a water molecule corresponding to the MIE for fixed θ and φ angles. We selected steps of 5° in θ and φ to scan the 3D MIE surface. In essence, we are "rolling" a nonvibrating water molecule against the nonvibrating nitrate ion infinitely slowly at a temperature of 0 K. For each of the optimized water−nitrate structures, we take the coordinates of the hydrogen atom closest to nitrate to create a hydrogen surface and the coordinates of the oxygen atom to create the oxygen surface. The hydrogen surface is displayed in Figure 6.

We found that for all pairs of angles (θ, φ) the H atom of the probe water molecule is closer to nitrate than the O atom of the probe. This is consistent with the envelope of negative ELP that surrounds the nitrate ion, including the regions above and below the nitrogen atom. Also consistent with the ELP contours is the fact that the probe water molecule comes close to the oxygen of nitrate in the region of the minimum-energy structures.[77,78] The probe molecule stays perceptibly further away from nitrate in the region above and below nitrogen. The H surface also shows a cusp corresponding to the water molecule rolling over and passing through a bidentate structure that is not a local minimum at the DFT(B3LYP)/6-311+G** level of theory but rather a transition state between two symmetry-equivalent minima with monodentate character.

Where the 3D H and O surfaces cut the molecular plane and the perpendicular plane is shown also in Figure 5. In Figure 5, we also show selected positions of the water molecule as it rolls over the nitrate surface. It can be seen that the H surface closely follows the ELP and isodensity contours around the terminal O atoms of nitrate, but it departs significantly from them in the bisecting region. Consistent with the H-donor type of bonding for the water molecule, the O surface remains further out than the H surface. The most striking features of the MIE surface can be seen in Figure 5 where the H surface lies close to the terminal oxygen atom but much further out in the bisecting region, including bulging out above and below the nitrogen atom. The shape of the MIE surface is consistent with the weaker ELP in these regions. It is worth remembering that the nitrate−water interaction potential, even if represented by a classical potential expression, combines the long-range electrostatic attraction/repulsion between nitrate and the partial atomic charges of water with the short-range repulsion (captured in the Lennard-Jones terms of the classical potential) to give rise to the trough around the solute. It should also be stressed that the MIE surface is a constrained surface of minimum interaction energy for fixed Euler angles θ and φ. The mode of representation of Figure 6 says nothing about the magnitude of the interaction energy or the existence of a local minimum-energy conformation. The most stable conformations are those of the monodentate binding structure with respect to the oxygen lone pairs in the molecular plane. As the water molecule rolls on the nitrate surface, the interaction energy decreases or increases depending on its position on the surface.

Also displayed in Figure 5 are the bond critical points (BCPs) between the nitrate and water subsystems as the water is rolled around the surface of the nitrate. BCPs are (3, −1) stationary points of the electron density of the total system. In the atoms-in-molecules theory of Bader,[80] surfaces with zero flux of electron density define the separate atoms of the system. BCPs are local maxima on those surfaces and can be thought of as the points at which solute and solvent just come into contact. Because a BCP surface defines (in terms of electron densities) the boundary between solute and solvent, it may be expected to bear some relationship to the most appropriate dielectric cavity surface. Bentley[81] has shown, using helium as a probe, that a surface defined by BCPs of helium−solute interactions strongly correlates with electron isodensity contours of the solute molecule. In the present case, the much stronger nitrate−water interaction distorts the BCP surface away from the isodensity surface of an isolated nitrate ion, generally in the direction of the water−hydrogen MIE surface. This is reasonable because the BCPs in this system generally join the proton involved in hydrogen bonding to the nearest atom in the nitrate. Note that the BCP surface lies inside the cavity surface defined by the radii of the nitrate ion in Table 2 or 3. This conforms to the general phenomenon that dielectric cavities are slightly larger than molecular dimensions, as illustrated by the 1.1−1.2 scaling of van der Waals radii for use in PCM.[13] Note also that no BCPs appear in the lower portion of the perpendicular plane of interaction in Figure 5 nor directly over the nitrogen nucleus. This is because even when the water is positioned in these locations the hydrogen is interacting with the nearest nitrate oxygen such that in the lower part of the Figure the BCPs are out of the plane of the Figure.

VII. Summary and Conclusions

In conclusion, we derived an empirical correlation of experimental hydration energies with quantum-derived descriptors, which yield species-specific radii that reproduce experimental energies with a high level of accuracy for a training set of oxoanions. The equations do not require any knowledge of the van der Waals radii; D_{X-O} effectively replaces the need for VdW radii and hybridization corrections. We demonstrated that our protocol is applicable to anions outside the training set, including systems for which solvation data are lacking. Application of the protocol to a wider class of oxoanions is in progress. We are currently considering the extension of the

approach described in this paper within the same protocol and/or using other solvation models to calibrate radii for other solutes (e.g., N_2, N_3, N_3^-, NO, N_2O, RNO, RNO_2, R_2SO, R_2SO_2, RSO_3^-, CN, CN^-, RCN, RS, RS^-, RO, RO^-, and ROR as well as cationic solutes and the conjugate acids of anions). Progress will be reported in future publications.

Acknowledgment. We thank Dr. Daniel M. Chipman (University of Notre Dame) for many helpful discussions. This work was supported by the U.S. Department of Energy, Environmental Management Science Program, and was performed, in part, using the Molecular Science Computing Facility (MSCF) in the William R. Wiley Environmental Molecular Sciences Laboratory at the Pacific Northwest National Laboratory. The MSCF is a national user facility funded by the Office of Biological and Environmental Research of the U.S. Department of Energy. The Pacific Northwest National Laboratory is a multiprogram national laboratory operated by Battelle Memorial Institute under contract no. DE-AC06-76RLO 1830. The Notre Dame Radiation Laboratory is supported by the Office of Chemical Sciences of the U.S. Department of Energy. This is contribution no. NDRL-4411.

Supporting Information Available: Geometries of the solutes listed in Table 1 optimized with and without the solvation model and their total free energies in water. This material is available free of charge via the Internet at http://pubs.acs.org.

References and Notes

(1) (a) Fessenden, W.; Meisel, D.; Camaioni, D. M. *J. Am. Chem. Soc.* **2000**, *122*, 3773. (b) Cook, A. R.; Dimitrijevic, N.; Dreyfus, B. W.; Meisel, D.; Curtiss, L. A.; Camaioni, D. M. *J. Phys. Chem. A* **2001**, *105*, 3658. (c) Meisel, D.; Camaioni, D. M.; Orlando, T. M. Radiation Chemistry in Nuclear Waste. In *Nuclear Site Remediation: First Accomplishments of the Environmental Management Science Program*; Eller, P. G., Heineman, W. R., Eds.; American Chemical Society: Washington, DC, 2000; p 342. (d) Camaioni, D. M.; Autrey, T. Thermochemical Kinetic Analysis of Mechanism for Thermal Oxidation of Organic Complexants in High Level Wastes; American Chemical Society: Washington, DC, 2000; p 299.

(2) Hehre, W. J.; Radom, L.; Schleyer, P. v. R.; Pople, J. A. *Ab Initio Molecular Orbital Theory*; Wiley & Sons: New York, 1986.

(3) Curtiss, L. A.; Redfern, P. C.; Raghavachary, K.; Pople, J. A. *J. Chem. Phys.* **1997**, *106*, 1063.

(4) Curtiss, L. A.; Redfern, P. C.; Raghavachary, K.; Pople, J. A. *J. Chem. Phys.* **1998**, *109*, 42.

(5) Curtiss, L. A.; Raghavachary, K.; Redfern, P. C.; Pople, J. A. *J. Chem. Phys.* **2000**, *112*, 7374.

(6) Hohenberg, P.; Kohn, W. *Phys. Rev. B* **1964**, *136*, 864.

(7) Kohn, W.; Sham, L. J. *Phys. Rev. A* **1965**, *140*, 1133

(8) Becke, D. *J. Chem. Phys.* **1993**, *98*, 1372. Becke, D. *J. Chem. Phys.* **1993**, *98*, 5648.

(9) Stevens, P. J.; Devlin, F. J.; Chabalowski, C. F.; Frisch, M. J. *J. Phys. Chem.* **1994**, *98*, 623.

(10) Tomasi, J.; Persico, M. *Chem. Rev.* **1994**, *94*, 2027.

(11) Cramer, J.; Truhlar, D. G. *Chem. Rev.* **1999**, *99*, 2161.

(12) Li, J. B.; Zhu, T. H.; Hawkins, G. D.; Winget, P.; Liotard, D. A.; Cramer, C. J.; Truhlar, D. G. *Theor. Chem. Acc.* **1999**, *103*, 9.

(13) Barone, V.; Cossi, M.; Tomasi, J. *J. Chem. Phys.* **1997**, *107*, 3210.

(14) Tissandier, M. D.; Cowen, K. A.; Feng, W. Y.; Gundlach, E.; Cohen, M. H.; Earhart, A. D.; Coe, J. V. *J. Phys. Chem. A* **1998**, *102*, 7787.

(15) Pliego, J. R., Jr.; Riveros, J. M. *Phys. Chem. Chem. Phys.* **2002**, *4*, 1622.

(16) Rinaldi, D.; Rivail, J. L. *Theor. Chim. Acta* **1973**, *32*, 57.

(17) Karelson, M.; Katritzki, A. R.; Szafran, M.; Zerner, M. C. *J. Org. Chem.* **1989**, *54*, 6030.

(18) Miertus, S.; Scrocco, E.; Tomasi, J. *Chem. Phys.* **1981**, *55*, 117.

(19) Zhu, T.; Li, J.; Hawkins, G. D.; Cramer, C. J.; Truhlar, D. G. *J. Chem. Phys.* **1998**, *109*, 9117.

(20) Klamt, A.; Schuurmann, G. *J. Chem. Soc., Perkin Trans. 2* **1993**, 799.

(21) Zhan, C.-G.; Chipman, D. M. *J. Chem. Phys.* **1998**, *108*, 177. Zhan, C.-G.; Chipman, D. M. *J. Chem. Phys.* **1998**, *109*, 10543. Zhan, C.-G.; Chipman, D. M. *J. Chem. Phys.* **1999**, *110*, 1611.

(22) Chipman, D. M. *J. Chem. Phys.* **2000**, *112*, 5558.

(23) Chipman, D. M. *Theor. Chem. Acc.* **2002**, *107*, 90.

(24) (a) Cancès, E.; Mennucci, B. *J. Chem. Phys.* **2001** *115*, 6130. (b) Mennucci, B.; Cammi, R.; Tomasi, J. *J. Chem. Phys.* **1998**, *109*, 2798.

(25) Cossi, M.; Scalmani, G.; Rega, N.; Barone, V. *J. Chem. Phys.* **2001**, *114*, 5691. Cossi, M.; Scalmani, G.; Rega, N.; Barone, V. *J. Chem. Phys.* **2002**, *117*, 43.

(26) Bondi, A. *J. Phys. Chem.* **1964**, *68*, 441. Atomic radii for H, C, N, O, and F are 1.2, 1.70, 1.55, 1.52, and 1.47 Å, respectively.

(27) Pauling, L. *The Nature of the Chemical Bond*; Cornell University Press: Ithaca, NY, 1960.

(28) Bonaccorsi, R.; Palla, P.; Tomasi, J. *J. Am. Chem. Soc.* **1984**, *106*, 1945.

(29) Orozco, M.; Luque, F. J. *Chem. Phys.* **1994**, *182*, 237.

(30) Bachs, M.; Luque, F. J.; Orozco, M. *J. Comput. Chem.* **1994**, *15*, 446.

(31) Stefanovich, V.; Truong, T. N. *Chem. Phys. Lett.* **1995**, *240*, 65.

(32) Rashin, A.; Namboodiri, K. *J. Phys. Chem.* **1987**, *91*, 6003.

(33) Cappelli, B.; Mennucci, B.; Silva, C. O. D.; Tomasi, J. *J. Chem. Phys.* **2000**, *112*, 5382.

(34) Aguilar, M. A.; Valle, F. J. O. d. *Chem. Phys.* **1989**, *129*, 439.

(35) Olivares del Valle, J.; Aguilar, M. A. *J. Comput. Chem.* **1992**, *13*, 115.

(36) Roux, B.; Yu, H. A.; Karplus, M. *J. Phys. Chem.* **1990**, *94*, 4683.

(37) Rick, S. W.; Berne, B. J. *J. Am. Chem. Soc.* **1994**, *116*, 3949.

(38) Miertus, S.; Bratos, J.; Trebaticka, M. *J. Mol. Liq.* **1987**, *33*, 139.

(39) Takahashi, O.; Sawahata, H.; Ogawa, Y.; Kikuchi, O. *J. Mol. Struct.: THEOCHEM* **1997**, *393*, 141.

(40) Chipman, D. M. *J. Chem. Phys.* **2002**, *116*, 10129.

(41) Chipman, D. M. *J. Phys. Chem. A* **2002**, *106*, 7413.

(42) Frisch, M. J.; Trucks, G. W.; Schlegel, H. B.; Scuseria, G. E.; Robb, M. A.; Cheeseman, J. R.; Zakrzewski, V. G.; Montgomery, J. A., Jr.; Stratmann, R. E.; Burant, J. C.; Dapprich, S.; Millam, J. M.; Daniels, A. D.; Kudin, K. N.; Strain, M. C.; Farkas, O.; Tomasi, J.; Barone, V.; Cossi, M.; Cammi, R.; Mennucci, B.; Pomelli, C.; Adamo, C.; Clifford, S.; Ochterski, J.; Petersson, G. A.; Ayala, P. Y.; Cui, Q.; Morokuma, K.; Malick, D. K.; Rabuck, A. D.; Raghavachari, K.; Foresman, J. B.; Cioslowski, J.; Ortiz, J. V.; Stefanov, B. B.; Liu, G.; Liashenko, A.; Piskorz, P.; Komaromi, I.; Gomperts, R.; Martin, R. L.; Fox, D. J.; Keith, T.; Al-Laham, M. A.; Peng, C. Y.; Nanayakkara, A.; Gonzalez, C.; Challacombe, M.; Gill, P. M. W.; Johnson, B. G.; Chen, W.; Wong, M. W.; Andres, J. L.; Head-Gordon, M.; Replogle, E. S.; Pople, J. A. *Gaussian 98*, revision A.7; Gaussian, Inc.: Pittsburgh, PA, 1998.

(43) Smith, B. J.; Hall, N. E. *J. Comput. Chem.* **1998**, *19*, 1482.

(44) Das, G. P.; Dudis, D. S. *J. Phys. Chem. A* **2000**, *104*, 4767.

(45) Ben-Naim, A. *J. Solution Chem.* **2001**, *30*, 475. Ben-Naim, A. *J. Phys. Chem.* **1978**, *82*, 782.

(46) Patterson, E. V.; Cramer, C. J.; Truhlar, D. G. *J. Am. Chem. Soc.* **2001**, *123*, 2025.

(47) Hydration free energies (ΔG_s*)[45] of neutrals (O_2, CO_2, NO_2, SO_2, ClO_2) were calculated from Henry's law constants available online from the NIST Chemistry WebBook[48] according to the equation $\Delta G_s^* = -RT \ln(K_h/0.987/0.0409)$ kcal/mol. The units of K_h are M/bar. The factors 0.987 atm/bar and 0.0409 M/atm (molar concentration of an ideal gas at $T = 298$ K and $P = 1$ atm) convert to M/M units. The ΔG_s* values for anions are derived from the free energies of formation (ΔG_f°) tabulated in Table 2. By definition, $\Delta G_f^\circ(H^+(aq)) = 0$. Therefore, $\Delta G_s^* = \Delta G_f^\circ(A^-(aq)) - \Delta G_f^\circ(A^-(g)) + \Delta G_f^\circ(H^+(g)) + \Delta G_s^\circ(H^+) - 1.89$ kcal/mol, where the last term converts from the gas-phase pressure standard state to the gas-phase concentration standard state, $\Delta G_s^\circ(H^+) = 264.0$ kcal/mol,[14] and following the ion convention, $\Delta G_f^\circ(H^+(g)) = 362.6$ kcal/mol.[53]

(48) *NIST Chemistry WebBook*; NIST Standard Reference Database Number 69; Linstrom, P. J., Mallard, W. G., Eds.; National Institute of Standards and Technology: Gaithersburg, MD, 2001; http://webbook.nist.gov.

(49) Some hydration free energies and electrode potentials used in this study are derived from *CODATA Key Values for Thermodynamics*; Cox, J. D., Wagman, D. D., Medvedev, V. A., Eds.; Hemisphere Publishing Corp.: New York, 1989; http://www.codata.org/databases/key1.html.

(50) Hickel, B.; Corfitzen, H.; Sehested, K. *J. Phys. Chem.* **1996**, *100*, 17186.

(51) Wardman, P. *J. Phys. Chem. Ref. Data* **1989**, *18*, 1637.

(52) Klaning, U. K.; Sehested, K.; Holcman, J. *J. Phys. Chem.* **1985**, *89*, 760.

(53) Bartmess, J. E. *J. Phys. Chem.* **1994**, *98*, 6420.

(54) Schwarz, H. A.; Dodson, R. W. *J. Phys. Chem.* **1989**, *93*, 409.

(55) *Lange's Handbook of Chemistry*, 13th ed.; Dean, J. A., Ed.; McGraw-Hill: New York, 1985.

(56) (a) Huie, R. E. *Radiat. Phys. Chem.* **1991**, *38*, 477. (b) Bonini, M. G.; Augusto, O. *J. Biol. Chem.* **2001**, *276*, 9749.

(57) Wilmarth, W. K.; Stanbury, D. M.; Byrd, J. E.; Po, H. N.; Chua, C.-P. *Coord. Chem. Rev.* **1983**, *51*, 155.

(58) Neta, P.; Huie, R. E. *J. Phys. Chem.* **1986**, *90*, 4644.

(59) Neta, P.; Huie, R. E.; Harriman, A. *J. Phys. Chem.* **1987**, *91*, 1606.

(60) Cotton, F. A.; Wilkinson, G. *Advanced Inorganic Chemistry*, 5th ed.; Wiley & Sons: New York, 1988.

(61) (a) Barone, V.; Cossi, M.; Tomasi, J. *J. Comput. Chem.* **1998**, *19*, 404. (b) Barone, V.; Cossi, M. *J. Phys. Chem. A* **1998**, *102*, 1995.

(62) (a) Cossi, M.; Mennucci, B.; Pitarch, J.; Tomasi, J. *J. Comput. Chem.* **1998**, *19*, 833. (b) Cammi, R.; Tomasi, J. *J. Comput. Chem.* **1995**, *16*, 1449.

(63) Cancès, E.; Mennucci, B. *J. Chem. Phys.* **2001**, *114*, 4744.

(64) Camaioni, D. M.; Dupuis, M. Submitted for publication.

(65) Krishnan, R.; Binkley, J. S.; Seeger, R.; Pople, J. A. *J. Chem. Phys.* **1980**, *72*, 650.

(66) Blaudeau, J.-P.; McGrath, M. P.; Curtiss, L. A.; Radom, L. *J. Chem. Phys.* **1997**, *107*, 5016.

(67) Kendall, R. A.; Apra, E.; Bernhold, D. E.; Bylaska, E. J.; Dupuis, M.; Fann, G. I.; Harrison, R. J.; Ju, J.; Nichols, J. A.; Nieplocha, J.; Straatsma, T. P.; Windus, T. L.; Wong, A. T. *Comput. Phys. Commun.* **2000**, *128*, 260.

(68) Chipman, D. M.; Dupuis, M. *HONDO-2002* computer code based on Dupuis, M.; Marquez, A. A.; Davidson, E. R. *HONDO-1995*; Quantum Chemistry Program Exchange; Indiana University: Bloomington, IN.

(69) (a) Singh, U. C.; Kollman, P. A. *J. Comput. Chem.* **1984**, *5*, 129. (b) Chirlian, L. E.; Francl, M. M. *J. Comput. Chem.* **1987**, *8*, 894. (c) Besler, B. H.; Merz, K. M.; Kollman, P. A. *J. Comput. Chem.* **1990**, *11*, 431. (d) Breneman, C. M.; Wiberg, K. B. *J. Comput. Chem.* **1990**, *11*, 361.

(70) Kosak-Channing, L. F.; Helz, G. R. *Environ. Sci. Technol.* **1983**, *17*, 145.

(71) Xidos, J. D.; Li, J.; Hawkins, G. D.; Liotard, D. A.; Cramer, C. J.; Truhlar, D. G. *HONDO/S-2.0*; University of Minnesota: Minneapolis, MN, 2000 (based on *HONDO-2000* by Dupuis, M.; Marquez, A.; Davidson, E. R. 2000).

(72) A reviewer pointed out that the atomic radii for X and O atoms (eqs 1 and 2) unavoidably depend on the nature of the charges, which are not a quantum mechanical observable and depend on the procedure chosen for their derivation. Therefore, that "the radius for atom X seems to be excessively enlarged" may be a consequence of the electrostatic potential charges used in the computational scheme. Furthermore, the reviewer mentioned that fitting to the quantum mechanical electrostatic potential tends to give exceedingly large charges for buried atoms.[73] We investigated various schemes and found that CHELPG charges and restrained electrostatic potential charges are negligibly different for the nitrate ion and for the tetrahedral perchlorate ion. Also, we note that charge schemes such as the Löwdin[74] and CM2 charges[75] on terminal oxygens calculated by the SM5 module of *HONDO 2002* are typically smaller than the electrostatic potential-derived charges (e.g., 40% smaller in the case of the nitrate ion). However, using these charges in eq 1 makes the oxygen radius in the nitrate ion just 0.06 Å larger, and we find that reducing the nitrogen radius by just 0.07 Å regains agreement of the calculated solvation energy with experiment. Therefore, we conclude that the unique characteristics of our protocol are a result of relating cavity radii to atomic charges and not the charge scheme used for deriving the atomic charges.

(73) Bayly, C. I.; Cieplak, P.; Cornell, W. D.; Kollman, P. A. *J. Phys. Chem.* **1993**, *97*, 10269.

(74) Löwdin, P.-O. *Adv. Quantum Chem.* **1970**, *5*, 185.

(75) Li, J.; Zhu, T.; Cramer, C. J.; Truhlar, D. G. *J. Chem. Phys.* **1999**, *111*, 885. Li, J.; Zhu, T.; Cramer, C. J.; Truhlar, D. G. *J. Phys. Chem. A* **1998**, *102*, 1820.

(76) While this work was in progress, a similar plot appeared in print: Hay, B. P.; Dixon, D. A.; Bryan, J. C.; Moyer, B. A. *J. Am. Chem. Soc.* **2002**, *124*, 182.

(77) Ebner, C.; Sansone, R.; Probst, M. *Int. J. Quantum Chem.* **1998**, *70*, 877.

(78) Wang, X. B.; Yang, X.; Wang, L. S.; Nicholas, J. B. *J. Chem. Phys.* **2002**, *116*, 561.

(79) Using the SS(V)PE model, an isodensity contour of 0.002e/cm^3 reproduces approximately the electrostatic solvation free energy of the nitrate ion in water. This contour is ∼1.6 Å from N above the molecular plane and ∼1.6 Å from O in the molecular plane compared to 2.4 and 1.52 Å, respectively, by our fitting procedure (Table 1). This contour is also less than ∼1.7 Å from N to the nearest critical points in the region above the molecular plane.

(80) Bader, R. W. F. *Atoms in Molecules: A Quantum Theory*; Oxford University Press: New York, 1990.

(81) Bentley, J. *J. Phys. Chem. A* **2000**, *104*, 9630.